

Z-99 High-resolution depth imaging with sparse inversion

JIANFENG ZHANG^{1,2} and KEES WAPENAAR¹

¹ Department of Geotechnology, Delft University of Technology, P.O. Box 5028, 2600 GA Delft, The Netherlands

² Institute of Geology and Geophysics, Chinese Academy of Sciences, Beijing 100029, China

Abstract

An imaging technique is developed which surpasses the resolution limitation prescribed by conventional seismic imaging methods. The high-resolution imaging is obtained by introducing a sparseness-constrained least-squares inversion into the imaging process of prestack depth migration. This is implemented by a proposed interference technique. The proposed method aims to image a small local region with a higher resolution. It should be applied following a conventional depth imaging if a higher resolution is needed in a target zone rather than replacing the conventional depth imaging for the entire medium. A synthetic example demonstrates the significant improvement of the resolution by the proposed scheme.

Introduction

Some reservoirs consist of stacked sheet sands, the thickness of which is frequently less than one-fourth of the available seismic wavelength. A high-resolution imaging scheme is therefore important to improve understanding of these reservoirs and to optimize well placement. Deconvolution (Robinson 1967) is the first approach to improve the resolution of seismic imaging. However, the usual assumptions about the wavelet phase and the statistics of the reflectivity restrict its applications in prestack imaging. Theoretically, non-linear inversion schemes based on optimal-fit-in-data-space (e.g. Jin *et al.* 1992) can achieve a high-resolution imaging beyond the limitation of the scale of the seismic wavelength. However, the computational cost for this kind of methods is too high to be applied in complicated structures, and the local minima and ill-posed problems require further study. The deconvolution and non-linear inversion methods represent two usual approaches to improve the resolution of seismic imaging by extending the frequency-band of seismic signals and by imaging using multiple reflected waves. The former is achieved in the deconvolution by the pre-whitening technique. This study, on the other hand, aims to improve the resolution by extending the frequency-band of the resulting reflection coefficients by following the prestack depth imaging approach.

Half-migration

Prestack depth migration is commonly accomplished by combining downward wavefield extrapolation with an imaging condition. If proper one-way propagators are used with a correct macro velocity model, prestack depth migration can put each event at its true location with the sharper focusing of reflected energy even in a strong laterally varying medium. This is essential for a high-resolution imaging in a complicated subsurface. Moreover, the different imaging conditions also have different effects on the resolution of the imaging. The correlation imaging condition produces wavelet stretch that degrades the resolution, whereas the deconvolution imaging condition yields band-limited reflection coefficients of the subsurface by removing the effect of the wavelet if the used source wavelet is exact. However, the exact estimation of the source wavelet is not easy. Since the wavelet exhibits space-variance resulting from varying velocities in an inhomogeneous medium but behaves time-invariant (if attenuation can be neglected), it will be more convenient to remove the effect of the source wavelet in the time-domain than in the depth-domain. Therefore, a half-migration technique, which can obtain a half-migrated shot gather expressed in the time-domain, is proposed based on inverse wavefield extrapolation. With $P^U(\mathbf{x}, \omega)$ denoting the inverse extrapolated shot gather in the space-frequency domain, and $T(\mathbf{x})$ and $A(\mathbf{x})$ the travel times for the source wavefield to arrive at each spatial grid-point and the corresponding amplitudes,

obtained by solving the eikonal and transport equations, the half-migrated shot gather in the depth-domain can be obtained as

$$\Phi(\mathbf{x}) = \int \left(P^U(\mathbf{x}, \omega) / A(\mathbf{x}) \right) \exp\{j\omega T(\mathbf{x})\} d\omega, \quad (1)$$

where j is the imaginary unit and $\mathbf{x} = (x, y, z)$ the Cartesian coordinate vector. We can then obtain the half-migrated shot gather $\Phi'(x, y, t)$, expressed in the time-domain, by replacing depth z with the related travel time $t = T(x, y, z)$ for each receiver position (x, y) . In order to avoid multipath arrivals, the travel time of the arrival with maximum energy, instead of first-arrival, will be used. Each trace in the half-migrated shot gather $\Phi'(x, y, t)$ can be understood as a record that would be measured at the source position (in the time-domain) when all reflectors along the depth direction at the related receiver position simultaneously excited the same wavelet (from the point of view of reciprocity). This half-migration technique keeps the wavelet invariant. We refer to it as ‘‘half-migration’’ because only half the propagation effects (in the travel times), i.e. from the subsurface reflectors to receivers, are removed. The high-resolution imaging scheme will be developed following this half-migrated result.

Interference technique

Provided that (intrinsic) attenuation is neglected, each trace in the half-migrated shot gather can be expressed in the frequency-domain as

$$\hat{\Phi}'(x, y, \omega) = \sum_{i=1}^n r_i S(\omega) \exp(-j\omega t_i), \quad (2)$$

where $S(\omega)$ is the spectrum of the source wavelet, t_i is the travel time from the point at the horizontal position (x, y) at the i th reflector (along the depth direction) to the source position, r_i is the reflection coefficient at the related point of the i th reflector, and n is total number of reflectors along the depth direction at the horizontal position (x, y) . If we further assume that all incidence angles are less than the corresponding critical angles (which is commonly assumed in seismic processing), all the reflection coefficients r_i will be real in eq.(2). By following optical interferometry, one of the arrivals, e.g. $a_1(\omega) = r_1 S(\omega) \exp(-j\omega t_1)$, is defined as the reference arrival. This reference arrival can be obtained by decomposing the corresponding trace using time-frequency spectral analysis or by decomposing the related half-migrated shot gather using generalized Randon transform. Then, we define the interference between the reference arrival with the related trace as follows:

$$j(\hat{\Phi}' \cdot a_1^* - \hat{\Phi}'^* \cdot a_1) = 2a_1 a_1^* \sum_{i=2}^n (r_i / r_1) \sin[\omega(t_i - t_1)]. \quad (3)$$

Eq.(3) gives an equation for unknown relative reflection coefficients $\bar{r}_i = r_i / r_1$. Instead of solving eq.(3) by the discrete Fourier series (considering ω as a variable), which will again produce band-limited reflection coefficients, a sparse inversion is introduced to solve eq.(3). This sparse inversion represents an alternative imaging algorithm in comparison with the correlation and deconvolution imaging conditions used in conventional depth migrations.

Sparse inversion

With \mathbf{R} denoting the unknown relative reflection series of all \bar{r}_i , eq.(3) can be rewritten as

$$\mathbf{\Gamma R} = \mathbf{Y}. \quad (4)$$

Its least-squares solution reads

$$\mathbf{R} = (\mathbf{\Gamma}^T \mathbf{\Lambda}^T \mathbf{\Lambda} \mathbf{\Gamma} + \mathbf{W})^{-1} \mathbf{\Gamma}^T \mathbf{\Lambda}^T \mathbf{\Lambda} \mathbf{Y}, \quad (5)$$

where \mathbf{W} is a real-valued diagonal matrix whose elements are determined by the regularized mode for overcoming non-uniqueness of the solution, and $\mathbf{\Lambda}$ is a real-valued diagonal matrix whose elements denote the weight factors for different frequencies. If Gaussian regularization is imposed, a smoothed solution is obtained from eq.(5). This smoothed solution again represents band-limited reflection coefficients without a significant improvement of the resolution. If Cauchy regularization, as proposed by Sacchi and Ulrych (1996), is introduced to the least-squares problem, a sparse solution, i.e. the solution that is able to satisfy the data with the smallest number of reflection events, can be obtained. This sparse

solution represents a higher-resolution result in the time-domain. Note that it is necessary to map the resulting high-resolution reflection series from the time-domain to the depth-domain for common-depth-point stacking.

If some arrivals, which do not result from the target zone of interest, are muted in advance, the number of the unknown reflection coefficients can be much reduced. As a result, the solution of eq.(4) becomes easy and a more stabilized result can be obtained from eq.(5). Owing to the small travel time differences between those arrivals included in eq.(2) in this case, two additional benefits are also achieved. In particular the time-variance of the wavelet due to (intrinsic) attenuation can be neglected, and the amplitude $A(\mathbf{x})$ in eq.(1) can be taken as a constant. Thus, the calculation of amplitudes by solving the transport equation can be omitted in the half-migration processing. We therefore prefer to get a higher-resolution imaging in a local interested target zone by following this muting processing. Many techniques, e.g. Radon transform and time-frequency spectral analysis, can be used to decompose and mute the uninteresting events. It should be pointed out that the reference arrival does not need to be a reflection resulting from the target zone of interest. A time-shift technique can be used if the travel time difference is too large between the reference arrival and the interested reflection events.

Numerical examples

A 2-D synthetic seismic experiment is designed to test the proposed high-resolution imaging scheme. The subsurface velocity model is shown in Fig. 1. Since the research on the decomposition of reflection events is beyond the scope of this paper, we like to put a flat reflector well separated from the thin sands and not include other curved reflectors in this model. Thus, the experiment can focus on testing the proposed high-resolution imaging scheme. Shot records with shots moving from -120m to 120m and a shot interval of 40m are generated by an acoustic finite-difference scheme with a wavelet with a peak frequency of 20Hz, as the solid line shown in Fig. 2. The explicit operator scheme (Zhang *et al.* 2001) is used in the half-migration processing with a horizontal spacing of 20m and a vertical step of 4.33m.

The common-depth-point stacked section together with two conventional prestack depth migration results are shown in Fig. 3. The same explicit operator scheme and the same data set are used in conventional prestack depth migration with both the exact and approximated wavelets shown in Fig. 2. From Fig. 3(a) we find that the effect of the source wavelet is almost fully removed and the frequency-band of the reflection coefficients is extended. It is also observed that the peaks of the reflection series lie exactly on the interfaces of the thin sands with correct polarity. The flat bottom of the lowest sand is ambiguous in Figs 3(b) and 3(c), whereas it is visible in Fig. 3(a). As compared with Fig. 3(a), the shapes of the sands are inaccurate in Fig. 3(b) although an exact wavelet is used, and even poorer in Fig. 3(c) in spite of a not too bad estimation of the source wavelet. Comparing three results in Fig. 3, we also find that the proposed high-resolution imaging scheme efficiently suppresses the coherent noise originated from the internal multiples. The internal multiples included in the shot records explain that the reflection coefficients at parts of the reflectors are a little lower in Fig. 3(a). These comparisons demonstrate the quality of the proposed scheme.

Conclusions

An imaging technique for improving the resolution of thin layers has been presented. The proposed scheme needs to be used after applying a decomposition algorithm, e.g. a Radon transform or time-frequency spectral analysis, which helps to obtain a decomposed signal event and to mute reflections resulting from reflectors other than the interested target zone. Not any stochastic assumption is introduced in the proposed high-resolution imaging scheme; moreover, no source wavelet is required. The proposed scheme should be used following a conventional depth imaging if a higher resolution is needed in a target zone rather than replacing the conventional imaging schemes for the entire medium.

Acknowledgements

The first author J. Zhang thanks the Netherlands Research Centre for Integrated Solid Earth Science for supporting his research fellowship at Delft University of Technology.

References

Jin S., Madariaga R., Virieux J. and Lambare G. 1992. Two dimensional asymptotic iterative elastic inversion. *Geophys. J. Int.* 108, 575–588.

Robinson E. 1967. Predictive decomposition of time series with application to seismic exploration. *Geophysics* 32, 418-484.

Sacchi M. D. and Ulrych T. J. 1996. Estimation of the discrete Fourier transform- A linear inversion approach. *Geophysics* 61, 1128-1136.

Zhang J., Verschuur D. J. and Wapenaar, C. P. A. 2001. Depth migration of shot records in heterogeneous, transversely isotropic media using optimum explicit operators. *Geophysical Prospecting* 49, 287-299.

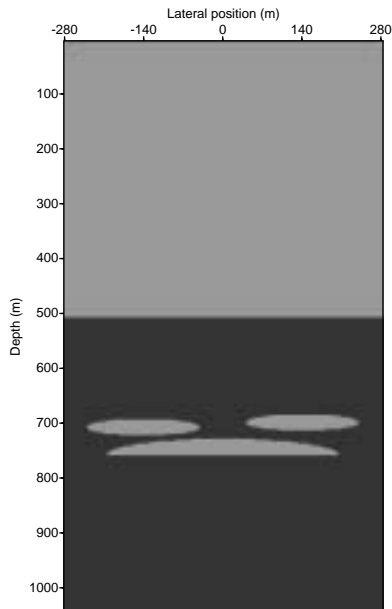


Fig.1. Subsurface velocity model with several thin sands. The maximum thickness of each of the sands is 30m. The light shade (including the sands) denotes a velocity of 2200m/s and the dark shade denotes a velocity of 3400m/s.

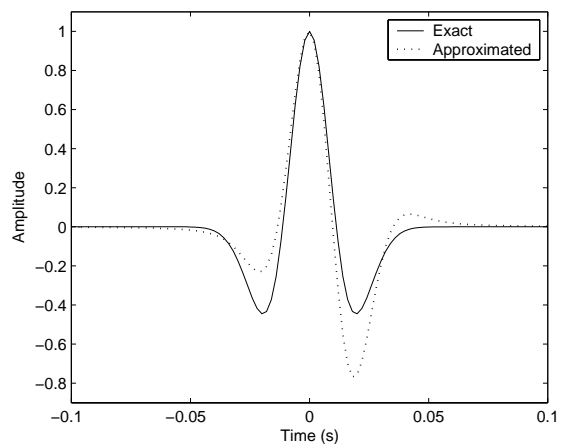


Fig.2. Exact and approximated source wavelets. The synthetic data set is generated using the exact wavelet denoted by the solid line. The peak frequency of both wavelets is 20Hz.

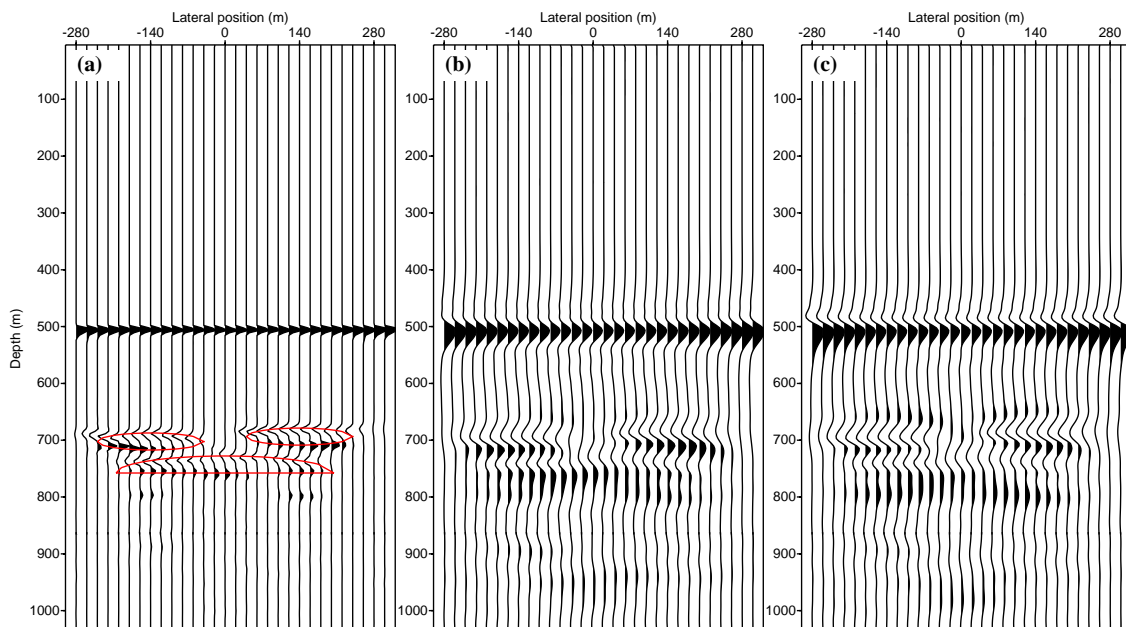


Fig.3. High-resolution imaging together with two conventional prestack depth migration results. (a) is obtained by the proposed scheme, (b) and (c) are the results of conventional prestack depth migration obtained using the exact and approximated wavelets, respectively. In total 7 shot gathers with shots moving from -120m to 120m and a shot interval of 40m are applied. The solid lines in (a) denote the interfaces of the three sands.